Available online at website: https://journal.bcrec.id/index.php/bcrec

Bulletin of Chemical Reaction Engineering & Catalysis, 21 (4) 2026, 863-876

Original Research Article

Eco-Friendly Activation of Fe_2O_3/GSBA-15 Using Tamarindus indica Pulp Extract for Enhanced Adsorptive Removal of Methylene Blue and Methyl Orange from Contaminated Water

Maria Ulfa*, Youlanda Jesiva Alba, Nurma Yunita Indriyanti, Nanik Dwi Nurhayati, Agung C. Saputro

Chemistry Education Study Program, Faculty of Teacher Training and Education, Sebelas Maret University, Jl. Ir. Sutami 36A Surakarta 57126, Indonesia.

Received: 31th May 2026; Revised: 29th July 2026; Accepted: 22th August 2026
Available online: 28th August 2026; Published regularly: December 2026

Abstract

In this study, a sustainable mesoporous silica material was synthesized using gelatin as a co-template (GSBA-15), followed by the incorporation of iron oxide (Fe_2O_3) to enhance its adsorption performance toward methylene blue (MB) and methyl orange (MO). *Tamarindus indica* pulp extract (TIE) was employed as a natural and environmentally benign activating agent, providing organic functionalities that facilitated material synthesis and surface modification. The adsorption performance of the synthesized materials, namely GSBA-15 and Fe_2O_3/GSBA-15-TIE, was evaluated using UV–Vis spectrophotometry. Under optimal adsorption conditions, the maximum adsorption capacities for MB were 176.062 and 183.497 $mg.g^{-1}$ for GSBA-15 and Fe_2O_3/GSBA-15-TIE, respectively. For MO, the corresponding adsorption capacities were 15.582 and 16.000 $mg.g^{-1}$. Kinetic studies revealed that the adsorption of both dyes was best described by the pseudo-second-order model, suggesting that chemisorption played a dominant role in the adsorption process. The enhanced adsorption performance of Fe_2O_3/GSBA-15-TIE compared with pristine GSBA-15 demonstrates the beneficial effects of iron oxide incorporation and TIE activation. These findings highlight the potential of Fe_2O_3/GSBA-15-TIE as a sustainable and efficient adsorbent for dye removal in wastewater treatment applications.

Keywords: Adsorption; Mesoporous Silica; Gelatin; Iron Oxide; Tamarindus indica

How to Cite: Ulfa, M., Alba, Y. J., Indriyanti, N. Y., Nurhayati, N. D., Saputro, A. C. (2026). Eco-Friendly Activation of Fe_2O_3/GSBA-15 Using Tamarindus indica Pulp Extract for Enhanced Adsorptive Removal of Methylene Blue and Methyl Orange from Contaminated Water. *Bulletin of Chemical Reaction Engineering & Catalysis*, 21 (4), 863-876. (DOI: 10.9767/bcrec.20757)

Permalink/DOI: https://doi.org/10.9767/bcrec.20757

1. Introduction

The water crisis is a difficult problem that has garnered political and scientific attention at the moment [1]. The textile sector uses a lot of water in its manufacturing processes, particularly when dyeing and finishing textile materials, which is the reason for this surge in activity. The negative effects of textile dyes may be caused by the processes used in textile dyeing [2]. Methylene blue (MB) and methyl orange (MO), generally referred to as persistent organic pollutants, are commonly used dyes in the textile industry [3]. These dyes' high molecular weight, low biodegradability, and strong chemical stability make them potentially harmful to the environment at low concentrations [4,5]. It is essential to remove water contamination using an efficient treatment method prior to its release into the stream of water. Membrane filtration, ion exchange, coagulation, advanced oxidation processes, and adsorption for dye removal are a few wastewater treatment methods. Because of its adaptability, versatility, and wide range of sorbents that it may be utilized with, adsorption is a good mechanism among a number of others [6].

* Corresponding Authors.
Email: mariaulfa@staff.uns.ac.id; ulfa.maria2015@gmail.com (M. Ulfa)

Mesoporous silica is a substance with porosity (pore size range of 2.5–15 nm) and a huge surface area (>1000 $m^2.g^{-1}$) [7]. Mesoporous silica has several benefits for adsorption, such as a wide surface area, consistent pore size, low cost, and the capacity to replenish itself through adsorption [8]. Some research have all examined the mesoporous silica material's capacity to adsorb the organic dyes MB and MO by it's sufficiently great porositiy to allow for the entrapment of large dyes molecules [9]. Nevertheless, synthetic soft templates such as CTAB, P123, or F127 are required for the synthesis of mesoporous silica. These templates need a lot of chemicals to make, are costly, and have a low sustainability level [10]. This led to earlier studies combining synthetic templates with organic materials that are safe for the environment, including natural gelatin. In earlier publications [11–13], the usage of gelatin containing amine groups ($-NH_2$) that have a significant affinity to engage through hydrogen bonding with hydroxyl (OH) offers an advantage as a pore directing agent.

A variety of techniques have been developed to functionalize mesoporous silica, aiming to enhance its selectivity and adsorption capacity for organic contaminants. One promising approach involves incorporating iron oxides into mesoporous silica, forming composites that significantly improve adsorption properties for a range of pollutants [14]. Among the various strategies, activation is considered one of the most effective and straightforward methods to increase the concentration of functional groups on the silica surface. This process enhances the surface area covered by oxygen-containing groups, which are critical for effective pollutant adsorption [15]. Interestingly, while many activation methods are explored, the use of organic activation agents remains relatively underutilized. This gap in research has led to the exploration of tamarind pulp as a potential organic activator. Tamarind pulp is rich in tartaric acid, a dicarboxylic acid containing two carboxyl functional groups [16]. According to Cashin *et al.* [15], carboxyl groups are highly effective in enhancing the adsorption capacity of mesoporous silica, especially for dyes. This insight suggests that the integration of tamarind pulp extract could offer a novel and environmentally friendly approach to improving the performance of mesoporous silica in pollutant removal applications.

The efficiency of dye adsorption onto a solid adsorbent is governed by several interrelated physicochemical parameters, namely contact time, solution temperature, initial dye concentration, adsorbent dosage, solution pH, and adsorbent particle size, all of which must be optimized to achieve maximum removal performance [17]. Contact time determines the kinetic profile of the process, as adsorption typically proceeds rapidly during the initial period when abundant vacant active sites are available on the adsorbent surface, before gradually slowing as these sites become occupied and the system approaches equilibrium [18]. Temperature influences adsorption differently depending on the thermodynamic nature of the process an increase in temperature generally enhances chemisorption-dominated systems by increasing the surface activity and kinetic energy of the adsorbate, whereas it tends to reduce adsorption capacity in physisorption-dominated systems, since weaker adsorbate–adsorbent interactions are more easily disrupted at elevated temperatures [17,19]. The initial dye concentration acts as a driving force that overcomes mass transfer resistance between the aqueous and solid phases at low concentrations the ratio of available active sites to dye molecules is high, allowing near-complete removal, whereas at higher concentrations the fixed number of binding sites becomes saturated, typically lowering the removal efficiency despite an increase in the absolute amount adsorbed per unit mass [17,18]. Adsorbent dosage similarly affects the balance between removal efficiency and adsorption capacity, since increasing the adsorbent mass at a fixed dye concentration provides more available surface area and binding sites and thereby improves the percentage removal, but often results in a lower adsorption capacity per gram due to the unsaturation of additional sites [17,18].

Solution pH is widely regarded as one of the most influential parameters, as it governs both the surface charge of the adsorbent and the ionization state of the dye molecules cationic dyes such as MB are generally adsorbed more effectively under basic conditions, where the adsorbent surface becomes deprotonated and negatively charged, favoring electrostatic attraction, whereas anionic dyes such as MO are more readily adsorbed under acidic to near-neutral conditions, where a protonated adsorbent surface promotes electrostatic interaction with the anionic dye species [17,19]. Finally, adsorbent particle size affects the specific surface area available for adsorption, since smaller particle sizes generally increase the density of accessible active sites and shorten intraparticle diffusion pathways, thereby enhancing both the rate and capacity of adsorption [17].

Beyond these process parameters, recent literature has increasingly emphasized the development of sustainable and eco-friendly strategies for enhancing adsorbent performance. Green activation methods, which rely on plant-derived extracts rich in bioactive compounds such as phenolics, flavonoids, and organic acids, have

emerged as attractive alternatives to conventional chemical activating agents, since they introduce additional functional groups onto adsorbent surfaces without generating hazardous byproducts. For instance, surface functionalization using mango seed extract as a natural bioactive source has been shown to enhance the adsorption of organic dyes, including methylene blue, methyl orange, and crystal violet, onto metal oxide adsorbents by altering surface charge and introducing phenolic binding sites [36], supporting the rationale behind the use of Tamarindus indica pulp extract as a green activating agent for GSBA-15 in the present study.

In parallel, mesoporous silica-based materials continue to attract considerable research attention as versatile adsorbent platforms owing to their high surface area, tunable pore architecture, and amenability to surface modification. Recent studies have demonstrated that tailoring the particle size, pore diameter, and surface functional groups of mesoporous silica materials can substantially improve their adsorptive capacity toward both inorganic and organic pollutants, including cationic and anionic dyes, with nanosized mesoporous silica particles possessing favorable surface charge proving particularly effective for dye removal applications [20]. These findings reinforce the potential of gelatin-templated mesoporous silica frameworks, such as GSBA-15, as tunable and sustainable platforms for further functionalization through iron oxide incorporation and organic activation.

More broadly, dye-containing wastewater treatment technologies have continued to diversify in recent years, encompassing physical, chemical, biological, and advanced oxidation approaches, each with distinct advantages, limitations, and industrial applicability. Among these, adsorption remains one of the most extensively investigated and industrially favorable techniques owing to its operational simplicity, relatively low cost, high removal efficiency, and minimal generation of secondary pollutants compared with chemical and advanced oxidation processes [21]. This continued preference for adsorption-based technologies underscores the relevance of developing low-cost, sustainable, and high-performance adsorbents such as Fe_2O_3/GSBA-15-TIE for practical dye wastewater remediation.

The principal novelty of this work lies in the use of Tamarindus indica pulp extract (TIE) as a fully aqueous, room-temperature, non-hazardous organic activator for a gelatin-templated, iron oxide-doped mesoporous silica, a combination that has not previously been reported. Earlier bio-based activation strategies for silica or carbon-based adsorbents have generally relied either on harsh chemical activators, such as KOH activation of tamarind seed for Fe(III) adsorption, or on energy-intensive thermal processing, such as pyrolysis-derived tamarind seed biochar, both of which offset part of the environmental benefit that a bio-based source would otherwise provide [22]. Similarly, the only previously reported plant-extract activation of a dye-adsorbing metal oxide surface, using mango seed extract, was applied to enhance surface charge and introduce phenolic binding sites on a metal oxide adsorbent without addressing the sustainability of the silica synthesis route itself [23]. In contrast, TIE activation in the present study requires only aqueous extraction and ambient soaking, generates no hazardous byproducts, and is applied directly onto a mesoporous silica already synthesized through a green, gelatin-templated route, so that the sustainability benefit is realized at both the templating and the activation stages rather than at only one of them. Furthermore, unlike prior tamarind-based activators that were evaluated on carbon or metal-oxide supports in isolation, this study is the first to combine TIE activation with Fe_2O_3 doping on gelatin-templated mesoporous silica, demonstrating that the carboxyl and hydroxyl functionalities naturally present in TIE work synergistically with the Fe-based active sites to enhance adsorption of both cationic (MB) and anionic (MO) dyes, thereby establishing TIE as a viable, low-cost, and genuinely green alternative to conventional or partially green activating agents for dye-adsorbing mesoporous silica composites.

The objective of this research was to assess the adsorption capacity of mesoporous silica for the batch adsorption of MB and MO from textiles using gelatin co-template doped iron oxide and Tamarindus indica pulp activator. The characterization by means of an UV–Visible spectrophotometer, X-Ray Diffraction (XRD), Fourier Transform Infrared Spectroscopy (FTIR), Scanning Electron Microscope-Energy Dispersive X-Ray (SEM-EDX) methods. Additionally, in order to remove MB and MO from textile effluent, reaction condition contact time was adjusted. The adsorption mechanism was assessed using the adsorption kinetic model.

Between the two common iron oxide phases, Fe_2O_3 (hematite) was deliberately selected over Fe_3O_4 (magnetite) as the active dopant in this study. Hematite is the thermodynamically stable end product of iron oxidation under ambient, oxygen-rich conditions, whereas magnetite is metastable and spontaneously oxidizes toward Fe_2O_3 upon exposure to air or elevated temperature [24]. Consequently, Fe_2O_3 can be obtained reliably through a simple one-step calcination of the impregnated iron precursor in

air, as performed in this work, without the strict oxygen-free atmosphere and precisely controlled Fe^{2+}/Fe^{3+} molar ratio required to prevent partial oxidation to hematite or goethite during Fe_3O_4 synthesis [25]. This translates into lower reagent and processing cost, fewer synthesis steps, and better reproducibility, making Fe_2O_3 more compatible with the low-cost, green activation strategy pursued in this study. Nevertheless, the superparamagnetic character of Fe_3O_4, which allows a spent adsorbent to be recovered rapidly using an external magnet rather than by filtration or centrifugation, is a valuable practical advantage for adsorbent reuse [26]. This magnetic-separation benefit was not required for the present proof-of-concept study but is acknowledged as an important direction for future work, in which Fe_3O_4-doped GSBA-15 TIE composites could be developed to combine the adsorption performance demonstrated here with facile magnetic recovery and recyclability.

2. Materials and Method

2.1. Materials

Tamarindus indica pulp was purchased from Surabaya, Indonesia. Methanol (Merck), aquadest (Smart-Lab), hydrochloric acid (37%, Merck, MW 36.46 g.mol^{-1}), triblock copolymer Pluronic P123 (Sigma-Aldrich, MW 5750 g.mol^{-1}), commercial gelatin (Gelita, MW ≈ 90,000 g.mol^{-1}), tetraethyl orthosilicate (TEOS, Merck KGaA, MW 208.33 g.mol^{-1}), iron(III) chloride hexahydrate ($FeCl_3 \cdot 6H_2O$, MW 270.30 g.mol^{-1}), methylene blue (MB, Merck, MW 319.85 g.mol^{-1}), and methyl orange (MO, Merck, MW 327.33 g.mol^{-1}) were used without further purification.

2.2. Synthesis of GSBA-15 TIE

Mesoporous silica with gelatin as the co-template (GSBA-15) was prepared by following the previous study [10]. A total of 4.00 g (0.696 mmol) of Pluronic P123 and 0.04 g (4.4×10^{-7} mol) of commercial gelatin were dissolved in 19.5 mL of 37% HCl (≈8.55 g pure HCl, 0.234 mol) and 127 mL of distilled water. The mixture was stirred at 40 °C (500 rpm) for 3 h. Subsequently, 8.62 g (0.0414 mol) of TEOS was added, and stirring was continued for 24 h at the same temperature. The resulting sol was transferred into a Teflon-lined stainless-steel autoclave and subjected to hydrothermal treatment at 90 °C for 24 h. The solid product was filtered, washed with distilled water, and dried at 70 °C for 24 h, followed by a second drying step at 100 °C for 24 h. Finally, the dried powder was calcined at 550 °C for 5 h to remove the organic template, yielding GSBA-15. Furthermore, GSBA-15 powder was activated using tamarind pulp that had been extracted using methanol solvent refers to previous work [27] which tamarind pulp extract (TIE) was mixed with water in the ratio of 3:10 (% b/v). A total of 1.5 grams of GSBA-15 was added and soaked for 24 hours. Next, the solution was filtered and washed using 100 mL of distilled water. Filtrate was dried in an oven at 100 ^{0}C for 24 hours. This powder is called by GSBA-15 TIE.

2.3. Impregnation of Iron Oxide

$FeCl_3 \cdot 6H_2O$ (0.26968 g, 9.98×10^{-4} mol ≈ 1.00 mmol Fe) was dissolved in 8.9 mL of distilled water and stirred at 30 °C for 5 min. Then, 0.9 g of GSBA-15-TIE was added to the solution, and the mixture was sonicated at 30 °C for 2 h. The resulting solid was dried at 100 °C for 30 min and subsequently calcined in a furnace at 600 °C for 6 h to convert the impregnated iron precursor to Fe_2O_3, yielding Fe_2O_3/GSBA-15-TIE. 9.98×10^{-4} mol Fe corresponds to 4.99×10^{-4} mol Fe_2O_3 (0.0797 g), giving a nominal loading of ≈ 8.1 wt% Fe_2O_3 relative to the GSBA-15-TIE support (0.9 g), consistent with the low-iron-loading regime reported previously by the same group [14].

2.4 Characterizations

Functional groups were analyzed by Fourier Transform Infrared (FT-IR) spectroscopy within the range 4000-600 cm^{-1}. Crystal structures were characterized by X-Ray Diffraction (XRD). The morphology and elemental composition of Fe_2O_3/GSBA-15 TIE were investigated using Scanning Electron Microscope-Energy Dispersive X-Ray (SEM-EDX).

2.5 Dye Adsorption

To evaluate the adsorption kinetics and the effect of contact time (batch tests), adsorption of MB and MO was carried out by adding 50 mg of Fe_2O_3/GSBA-15 TIE into 200 mL of 50 mg/L MB/MO solution in a 250 mL round bottom flask. The resulting mixture was stirred at 200 rpm using a magnetic stirrer at seven different times (0, 10, 20, 30, 40, 50, 60 minute). After that, GSBA-15 was precipitated by centrifugation at 10,000 rpm for 5 min, and the final concentration of MB/MO in the supernatant was determined from optical adsorption 665 nm (MB) and 464 nm (MO). The adsorption capacity (q_t, the amount of adsorbed MB/MO per unit mass of adsorbent) of Fe_2O_3/GSBA-15 TIE was calculated by the following equation:

$$q_e = \frac{(C_o - C_e)V}{W} \quad (1)$$

where C_0 and C_e are the concentrations (mg L^{-1}) MB/MO at initial and at time t, respectively; V represents the volume of the solution (L); and W is the adsorbent mass (g). The removal efficiency

(*RE*%) was calculated by the following equation:

$$RE\% = \frac{(C_0 - C_e)V}{C_0} \times 100\% \quad (2)$$

3. Results and Discussion

3.1. Fourier Transform Infrared Spectroscopy (FTIR)

There were notable variations between the gelatin mesoporous silica samples before and after activation and impregnation, as indicated by the FTIR spectra (Figure 1, Table 1). In the GSBA-15 sample, the asymmetric and symmetric stretching vibrations of the siloxane (Si-O-Si) bond were observed at 1084.03 cm^{-1} and 798.56 cm^{-1}, respectively [13,28], while the silanol (Si-OH) bond appeared at 1635.69 cm^{-1}, exhibiting a high intensity of mesoporous ribbon nature (Figure 1a) [10]. Whereas, for Fe_2O_3/GSBA-15 TIE sample there is a broad spectrum in the hydroxyl (-OH) region at wave numbers 3372.04 cm^{-1}. This absorption band is associated with stretching vibrations of the Si-OH group. Iron oxide was identified as the source of the adsorption band at 571.00 cm^{-1} (Figure 1b). This indicates that that small quantity of Fe metal was successfully impregnated onto the GSBA-15 TIE material as a loading effect [28]. In addition, the wavenumbers of 1412.87 cm^{-1} indicate the band offered all of the bioorganic chemicals found in TIE [29]. The weak band at 1820.23 cm^{-1} is not attributable to a carbonyl (C=O) stretch, as this wavenumber is considerably higher than typical carbonyl stretching regions (esters ~1735-1750 cm^{-1} and carboxylic acids ~1700-1725 cm^{-1}). Instead, this band is assigned to the combination/overtone mode of the bulk Si-O-Si framework, commonly reported at 1850-1870 cm^{-1} in amorphous and mesoporous silica [30], further confirming that the amorphous silica network was retained after activation and impregnation.

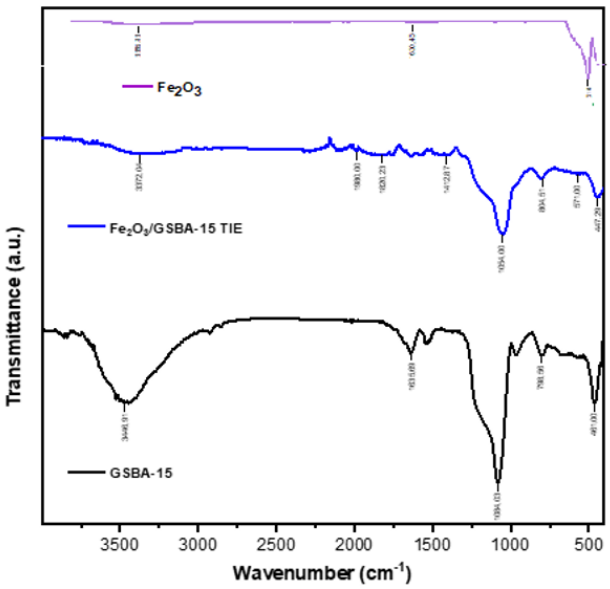

Figure 1. IR Spectra of (a) GSBA-15 and (b) Fe_2O_3/GSBA-15 TIE.

3.2. X-Ray Diffraction (XRD)

XRD analysis was subsequently performed on the GSBA-15 and Fe_2O_3/GSBA-15 TIE samples to determine the characteristics of the materials (Figure 2). The diffractogram's results indicate that the two samples' phases do not differ all that much. The existence of silica material GSBA-15 is shown by the amorphous phase shown in GSBA-15 (Figure 2a) and Fe_2O_3/GSBA-15 (Figure 2b) peak values with a wide curve, 23.49° and 22.46°, respectively. From these results, the 2θ peak value of GSBA-15 is in accordance with the standard SiO_2 diffraction data JCPDS No.29-0085. The Fe_2O_3/GSBA-15 TIE sample did not show any distinctive peaks of iron oxide or other Fe species, according to the diffractogram data. This suggests that iron oxide species could exist in GSBA-15 as amorphous particles or as finely scattered nano-dimensional particles (at least in one dimension) below the x-ray detection limit [33].

Table 1. FTIR analysis data from samples GSBA-15 and Fe_2O_3/GSBA-15 TIE.

Spectra	Wavenumber	Type Vibration	Reference
GSBA-15	3446.91	Stretching O-H	[31]
	1635.69	Stretching Si-OH	[28]
	1084.03	Asymmetric Stretching Si-O-Si	[10]
	798.56	Symmetric Stretching Si-O-Si	[13]
	461.00	Bending Si-O	[13]
Fe_2O_3/GSBA-15 TIE	3372.04	Stretching O-H	[31]
	1820.23	Combination/overtone Si-O-Si	[30]
	1412.87	Stretching O-C-O	[32]
	1054.00	Asymmetric Stretching Si-O-Si	[10]
	804.51	Symmetric Stretching Si-O-Si	[13]
	571.00	Vibration Fe-O	[28]
	447.29	Bending Si-O	[13]

Quantitative analysis was applied to get crystallite size and crystallinity degree of gelatin mesoporous silica before and after activation also impregnation change from 0.5555 nm to 0.3786 nm for crystal size and 66.07% to 83.67 % for crystallinity (Table 2). This is results show that activation process which uses TIE able to reduce the size of mesoporous silica indicate by lower peak intensity and width peak [34,35]. As we can see the diffractogram (Figure 2) where GSBA-15 silica has a higher peak than Fe_2O_3/GSBA-15 TIE with a sloping and wide peak.

Using SEM-EDX, the GSBA-15 and Fe_2O_3/GSBA-15 TIE samples were characterized. Figure 3 displays the morphology at various magnifications. The characteristic rod-like particle form of GSBA-15 silica, together with agglomeration with nearby particles, is evident in the surface morphology patterns of GSBA-15 and Fe_2O_3/GSBA-15 TIE. The pore structure of mesoporous silica may have an effect on its surface area. In order to maximize the adsorption of MB and MO by mesoporous silica, a greater surface area is obtained relative to the reduced pore size produced. Energy Dispersive X-ray Spectroscopy (EDX) coupled with Scanning Electron Microscopy (SEM) was used for characterization. This method enables for the qualitative assessment of chemical composition.

Table 2. Crystallinity result of GSBA-15 and Fe_2O_3/GSBA-15 TIE.

Sample	CD [%]	C [nm]
GSBA-15	66.0684	0.5555
Fe_2O_3/GSBA-15 TIE	83.6715	0.3786

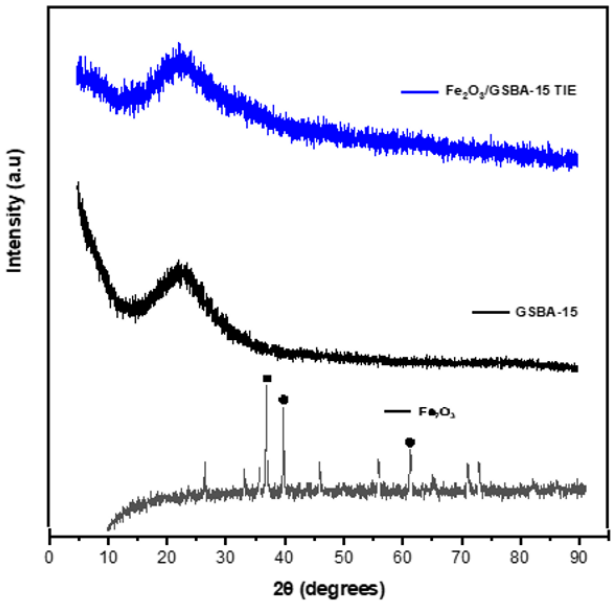

Figure 2. Diffractogram of (a) GSBA-15 and (b) Fe_2O_3/GSBA-15 TIE samples.

The findings indicate that 58.38% O and other elements are present in the mesoporous silica such as 40.36% Si for GSBA-15, then 49.92% O, 31.22% Si, 18.87% C, and 3,43% % Fe for Fe_2O_3/GSBA-15 TIE. The element Fe indicates

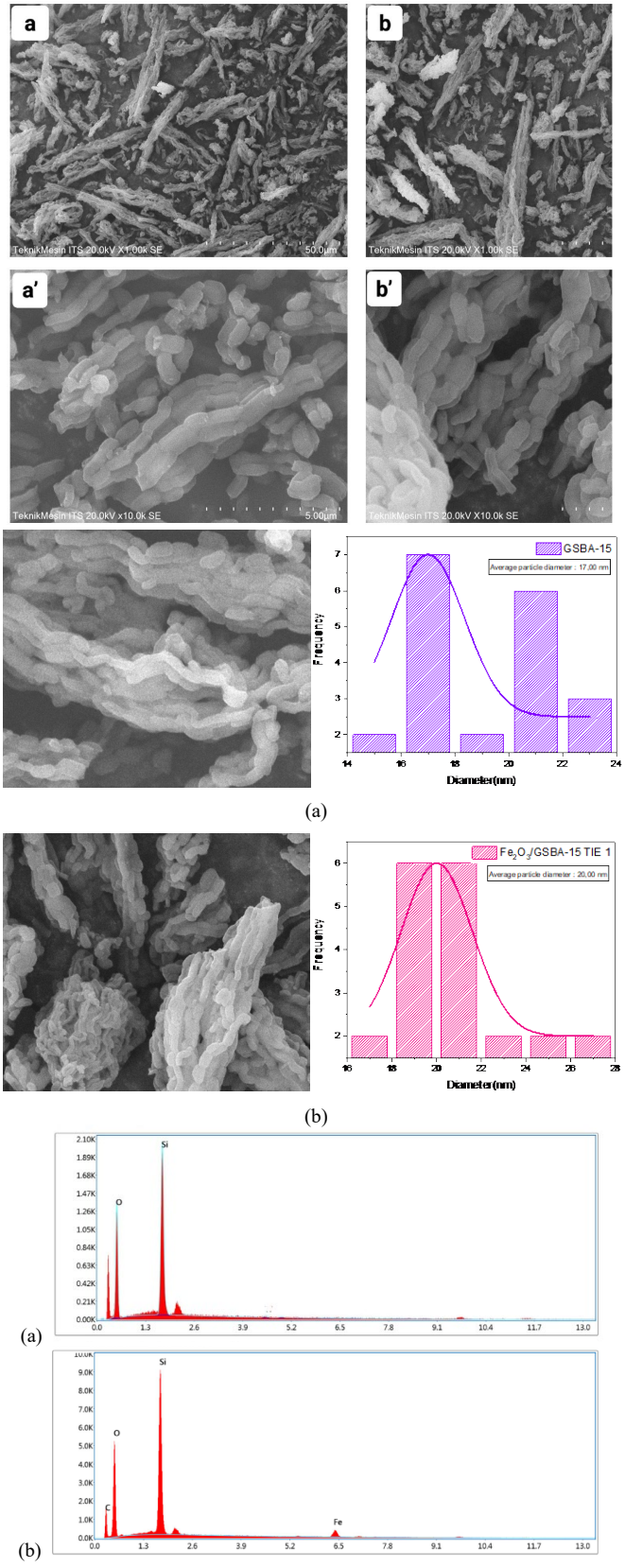

Figure 3. Low and high magnification SEM EDX images of (a, a') GSBA-15 and (b, b') Fe_2O_3/GSBA-15 TIE.

that iron oxide compounds are effectively immobilized on mesoporous silica.

3.3 Adsorption Ability Towards Organic Dyes Pollutant

The results of the adsorption against MB were computed (Table 3), and it is evident that adsorption takes place in the first 40 minutes with a significant capacity (±18 $mg.g^{-1}$) in all samples. Compared to the adsorption capacity value in the first 40 minutes, the adsorption capacity after 40 minutes tends to be stable (170.00 – 174.00 $mg.g^{-1}$). Every adsorbent sample will eventually achieve its maximal adsorption capacity before the capacity to adsorb drops. The best timing is at this point in time. On MB, the adsorption efficiency was 91.319%. With an average adsorption capacity of 15.79 mg/g, adsorption occurs in the first 30 minutes in all adsorbent samples, according to the adsorption data against MO (Table 4). This figure is significantly less than MB's adsorption capability. When comparing the adsorption capacity after 40 minutes to that of the first 30 minutes, fluctuations might be observed. On MO, the adsorption capacity only reaches 7.853%.

The adsorption process typically occurs in two distinct stages. During the initial phase (10–40 minutes), the rate of adsorption is relatively high due to the abundance of available active sites on the adsorbent surface, which readily interact with the empty adsorption sites of methylene blue (MB) and methyl orange (MO). However, as the process progresses, a noticeable deceleration occurs, signaling that the adsorption rate begins to slow down. This decline in pace corresponds to the attainment of equilibrium, where no significant changes in adsorption efficiency are observed [26]. This dynamic is clearly depicted in Figure 4, which illustrates the adsorption capacity over time.

Tamarind pulp extract, rich in organic acids such as tartaric acid, offers a unique activation mechanism. Tartaric acid, classified as a weak acid, only partially ionizes in solution, resulting in lower proton (H^+) concentrations compared to strong acids like hydrochloric acid (HCl) and sulfuric acid (H_2SO_4). While these stronger inorganic acids are typically more effective in enhancing the adsorption ability of materials, the organic acids in tamarind pulp interact differently with the mesoporous silica. Despite

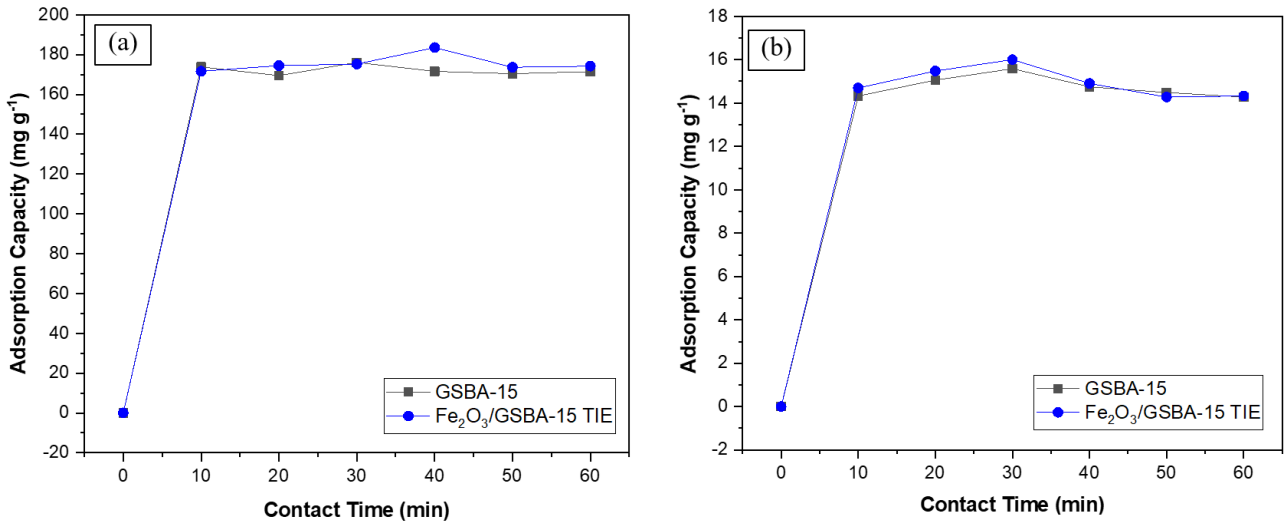

Figure 4. Adsorption capacity of (a) MB and (b) MO dye.

Table 3. Adsorption capacity for MB.

Contact Time (minutes)	Adsorption Capacity ($mg.g^{-1}$)	
	GSBA-15	Fe_2O_3/GSBA-15 TIE
0	0.00	0.00
10	173.76	171.61
20	169.46	174.41
30	176.06	175.22
40	170.00	183.49
50	170.34	173.60
60	171.40	174.13

Table 4. Adsorption capacity for MO.

Contact Time (minutes)	Adsorption Capacity ($mg.g^{-1}$)	
	GSBA-15	Fe_2O_3/GSBA-15 TIE
0	0.00	0.00
10	14.32	14.69
20	15.05	15.47
30	15.58	16.00
40	14.74	14.90
50	14.48	14.27
60	14.27	14.32

the relatively lower protonation capacity of tartaric acid, the extract still influences the adsorption activity, albeit to a lesser degree.

The best adsorption performance for MB was achieved with the Fe_2O_3/GSBA-15 TIE sample, which exhibited an adsorption capacity of 183.49 $mg.g^{-1}$, a modest increase of 7.43 $mg.g^{-1}$ over the pure GSBA-15 sample. Similarly, the Fe_2O_3/GSBA-15 TIE sample also demonstrated superior adsorption for MO, with a capacity of 16.00 $mg.g^{-1}$, showing a slight increase of 0.42 $mg.g^{-1}$ compared to the pure GSBA-15. While these increases may appear modest, they reflect the influence of the organic activating agent, which, as a weak acid, can protonate the active sites of the adsorbent, though in smaller amounts compared to stronger acids. Nevertheless, the use of tamarind pulp extract (TIE) presents a distinct advantage. Unlike conventional inorganic activating agents, TIE is more environmentally friendly, offering a sustainable alternative without introducing additional pollutants during the material synthesis process. This highlights the potential of TIE as a green activation agent in the development of mesoporous silica composites for pollutant removal.

3.4 Adsorption Mechanism of MB and MO onto Fe_2O_3/GSBA-15 TIE

The markedly higher uptake of MB relative to MO can be rationalized by the electrostatic interaction between the dye molecules and the adsorbent surface. Under the near-neutral aqueous conditions used in this study, the silanol (Si-OH) and Fe-OH groups on the GSBA-15 and Fe_2O_3/GSBA-15 TIE surfaces partially deprotonate to $Si\text{-}O^-$ and $Fe\text{-}O^-$, giving the adsorbent a net negative surface charge. MB carries a delocalized positive charge across its phenothiazine ring system, so it is electrostatically attracted toward these negatively charged oxygen sites, allowing strong and favorable ion-pairing at the interface. MO, in contrast, is an anionic dye whose negative charge is concentrated on the terminal sulfonate ($-SO_3^-$) group this charge distribution places MO in electrostatic repulsion with the deprotonated surface, which largely accounts for its much lower adsorption capacity. Whatever MO adsorption does occur is instead attributed to weaker, non-electrostatic contributions, such as hydrogen bonding between the azo and amine nitrogens of MO and surface hydroxyl groups, together with limited electrostatic attraction toward the comparatively few protonated $Fe\text{-}OH_2^+$ sites and exposed Fe^{3+} Lewis-acid centers on the Fe_2O_3 nanoparticles.

Molecular size and charge distribution further reinforce this preferential uptake. MB is a relatively compact, planar cation with a molecular weight of 319.85 $g.mol^{-1}$, and its positive charge is delocalized over the whole thiazine ring, enabling close and efficient contact with the pore-wall surface without significant steric hindrance. MO, although of comparable molecular weight (327.33 $g.mol^{-1}$), possesses a more extended structure due to the bulky, hydrated sulfonate group, which increases its effective hydrodynamic size and can partially hinder access to the narrower mesopores of GSBA-15 and Fe2O3/GSBA-15 TIE. Since electrostatic repulsion and steric bulk act in the same direction for MO, both factors combine to lower its adsorption capacity relative to MB, even though the mesostructure itself is wide enough to accommodate both dyes.

At the surface-interaction level, incorporation of Fe_2O_3 nanoparticles introduces additional Fe-OH groups and coordinatively unsaturated Fe^{3+} centers that can engage in inner-sphere complexation with the nitrogen and sulfur heteroatoms of the dye molecules, supplementing the silanol-based interactions already present on GSBA-15. TIE activation contributes a further layer of surface functionality: the carboxyl and hydroxyl groups derived from tartaric acid increase the density of oxygenated functional groups on the silica surface, providing additional hydrogen-bond acceptor sites and, upon deprotonation, additional negatively charged sites that specifically favor MB electrostatic docking. Together, these complementary silanol, Fe-OH, and TIE-derived carboxyl/hydroxyl sites explain why Fe_2O_3/GSBA-15 TIE consistently outperforms pristine GSBA-15 for both dyes, with the improvement being proportionally larger for MB, whose adsorption mechanism is dominated by these newly introduced negatively charged and coordinating sites.

Consistent with the pseudo-second-order kinetics discussed below, which points to chemisorption as the dominant mechanism, the active sites governing this process are the finite population of surface functional groups capable of forming coordinate or ionic bonds, or hydrogen bonds, with the adsorbate: the Si-OH/$Si\text{-}O^-$ groups of the silica framework, the Fe-OH/$Fe\text{-}O^-$ groups and Fe^{3+} centers introduced by iron oxide impregnation, and the carboxyl/hydroxyl groups contributed by TIE activation. The two-stage adsorption profile observed for both dyes reflects the behavior of this finite site population: during the initial 10-40 minutes, adsorption proceeds rapidly because abundant vacant active sites are readily accessible at and near the external particle surface, whereas the subsequent plateau reflects progressive saturation of these sites and slower diffusion of the dye molecules toward less

accessible sites within the mesopore interior. Because MB and MO are adsorbed onto the same population of active sites, the pronounced difference in their respective adsorption capacities is governed primarily by how favorably each dye's charge and size match those sites, as described above, rather than by a difference in the total number of sites available. The smaller crystallite size and higher crystallinity of Fe2O3/GSBA-15 TIE relative to pristine GSBA-15 (Table 2) are also consistent with a more ordered surface bearing a greater density of accessible hydroxyl and oxide active sites, reinforcing the higher adsorption capacities obtained for the activated, iron oxide-loaded material.

3.5 Adsorption Kinetic

The pseudo-first-order model based on the Lagergren equation and the pseudo-second-order model based on the Ho and McKay equation were used to describe the adsorption kinetics of MB and MO onto GSBA-15 and Fe_2O_3/GSBA-15 TIE. The linearized forms of the Lagergren pseudo-first-order [36] and Ho and McKay pseudo-second-order [37] kinetic models are given, respectively, by:

$$\log (q_e - q_t) = \log q_e - \frac{k_1}{2.303} t \quad (3)$$

$$t/q_t = \frac{1}{k_2 q_e^2} + \frac{t}{q_e} \quad (4)$$

where q_e and q_t (mg.g^{-1}) are the amounts of dye adsorbed at equilibrium and at time t (min), respectively; k_1 (min^{-1}) is the Lagergren pseudo-first-order rate constant; and k_2 (g.mg^{-1}.min^{-1}) is the Ho and McKay pseudo-second-order rate constant.

To demonstrate the kind of adsorption that takes place, adsorption kinetics calculations have been performed (Tables 5-6). Higher R^2 values are seen for both adsorption on MB and MO at pseudo second order in all samples (Figures 5-8). The pseudo second-order reaction kinetics model indicates that adsorption reactions involve chemisorption processes [38]. Chemical adsorption also known as chemisorption occurs by substantial electron sharing or transfer between the adsorbent and adsorbate surfaces to create covalent or ionic bonds. When adsorbate molecules are adsorbed on the adsorbent surface through valence bonds, they form a monolayer [39]. In chemical adsorption, the amount of adsorbed substance is directly proportional to the number of active nuclei of the adsorbent that can

Table 5. MB adsorption kinetics model parameters.

Sample	Pseudo 1st Order				Pseudo 2nd Order			
	R^2	$q_{e,Cal}$	k_1	$q_{e,Exp}$	R^2	$q_{e,Cal}$	k_2	$q_{e,Exp}$
GSBA-15	0.086	22.760	0.034	176.062	0.999	0.001	0.006	176.062
Fe_2O_3/GSBA-15 TIE	0.237	39.607	0.033	183.497	0.998	3329.575	0.006	183.497

Table 6. MO adsorption kinetics model parameters.

Sample	Pseudo 1st Order				Pseudo 2nd Order			
	R^2	$q_{e,Cal}$	k_1	$q_{e,Exp}$	R^2	$q_{e,Cal}$	k_2	$q_{e,Exp}$
GSBA-15	0.080	3.230	0.026	15.582	0.998	0.960	0.070	15.582
Fe_2O_3/GSBA-15 TIE	-0.049	3.248	0.196	16.000	0.996	0.934	0.070	16.000

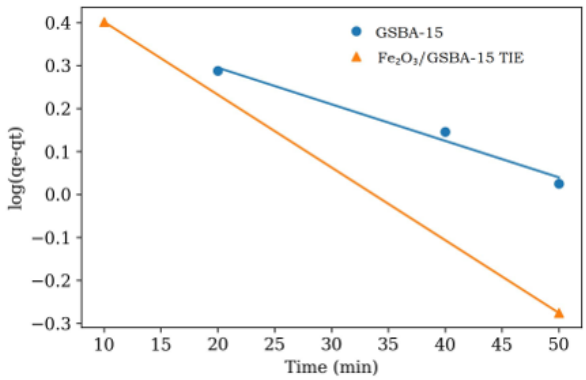

Figure 5. Pseudo-first-order kinetic plots for the adsorption of methylene blue onto GSBA-15 and Fe_2O_3/GSBA-15 TIE.

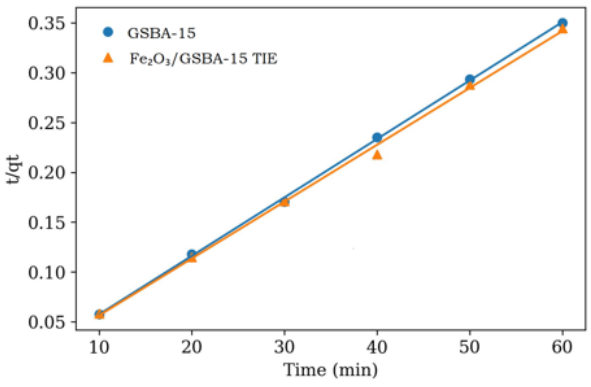

Figure 6. Pseudo-second-order kinetic plots for the adsorption of methylene blue onto GSBA-15 and Fe_2O_3/GSBA-15 TIE.

react with the adsorbate. The results of this adsorption kinetics determination indicate that the type of adsorption that occurs in the methylene blue and methyl orange adsorption process is chemical adsorption. The pseudo second-order kinetics model is hence the relevant kinetics.

To place the performance of Fe_2O_3/GSBA-15 TIE in the context of previously reported adsorbents, Table 7 summarizes the maximum adsorption capacity (Q_{max}) and the operating conditions (pH, adsorbent dose, and contact time) reported for several dye adsorbents in the literature, including magnetic- and iron oxide-based composites. Compared with pristine GSBA-15, Fe_2O_3 doping increased the MB and MO capacities of GSBA-15 TIE by only a modest margin, and both values remain lower than several magnetic carbon-based adsorbents such as the Fe_3O_4-doped watermelon shell activated carbon reported by Rajendran *et al.* [6]. Nevertheless, Fe_2O_3/GSBA-15 TIE remains competitive with other iron oxide-modified mesoporous silicas, such as the Fe-γ-CS-SBA-15 composite [40], while offering a simpler, one-step, fully aqueous and room-temperature activation route. This comparison indicates that further tuning of the Fe_2O_3 loading, particle dispersion, and support porosity could narrow the performance gap with higher-capacity magnetic adsorbents, consistent with the future-work direction toward Fe_3O_4-doped composites noted above.

Figure 9 illustrates the proposed adsorption mechanisms of methylene blue (MB) and methyl orange (MO) on the Fe_2O_3/GSBA-15 composite,

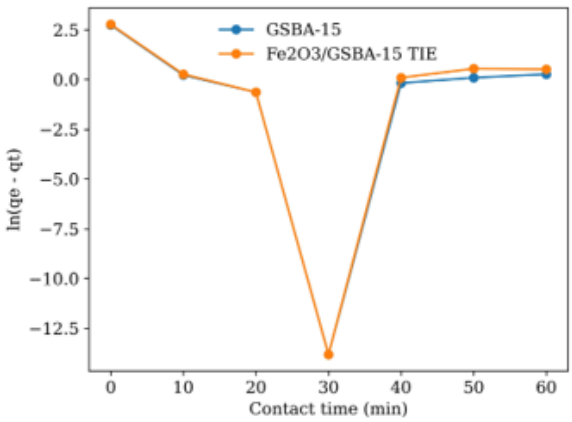

Figure 7. Pseudo-first-order kinetic plots for the adsorption of methyl orange onto GSBA-15 and Fe_2O_3/GSBA-15 TIE.

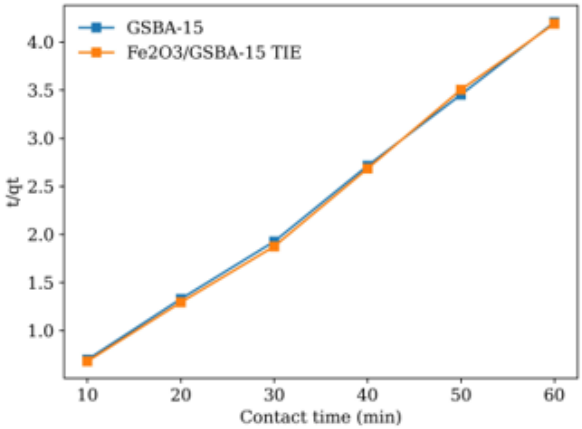

Figure 8. Pseudo-second-order kinetic plots for the adsorption of methyle orange onto GSBA-15 and Fe_2O_3/GSBA-15 TIE.

Table 7. Comparison of adsorption capacity and operating conditions with previously reported adsorbents.

Adsorbent	Dye	pH	Dose	Contact time (min)	Q_{max} (mg.g^{-1})	Ref.
Fe_2O_3/GSBA-15 TIE (this study)	MB	unadjusted (natural)	0.25 g.L^{-1}	40	183.497	This study
Fe_2O_3/GSBA-15 TIE (this study)	MO	unadjusted (natural)	0.25 g.L^{-1}	30	16.000	This study
GSBA-15 (undoped, this study)	MB	unadjusted (natural)	0.25 g.L^{-1}	40	176.062	This study
GSBA-15 (undoped, this study)	MO	unadjusted (natural)	0.25 g.L^{-1}	30	15.582	This study
Magnetic activated carbon/watermelon shell (MWMSC)	MB	6.0	100 mg	60	303.30	[6]
Magnetic activated carbon/watermelon shell (MWMSC)	MO	3.0	100 mg	40	345.70	[6]
Activated carbon/Fe_3O_4 nanocomposite (ACL/Fe_3O_4)	CV	9.0	–	–	35.3	[26]
Fe-modified high-silica fly ash mesoporous silica (MSM)	MB	9.0	2 g.L^{-1}	150	115.34	[18]
Fe-γ-CS-SBA-15 (iron oxide/chitosan-modified SBA-15)	MB	–	–	–	176.70	[40]

highlighting the synergistic contribution of multiple intermolecular interactions. For methylene blue, adsorption is primarily facilitated through hydrogen bonding between the silanol (Si–OH) groups of GSBA-15 and the nitrogen-containing functional groups of MB, complemented by π–π interactions involving the aromatic conjugated structure of the dye and the Fe_2O_3 active sites. In addition, electrostatic attraction between the positively charged dimethylammonium group ($–N^+(CH_3)_2$) of MB and negatively polarized oxygen species on the Fe_2O_3 surface further strengthens the adsorption process. The coexistence of these interactions promotes firm anchoring of MB molecules onto the adsorbent surface, thereby enhancing the overall adsorption capacity.

In other side, the adsorption of methyl orange proceeds through a distinct yet complementary interaction pathway. Hydrogen bonding occurs between the amino group of MO and the surface silanol groups of GSBA-15, while π–π interactions arise from the aromatic backbone of MO and the Fe_2O_3 surface. Electrostatic attraction is also expected between the negatively charged sulfonate group ($–SO_3^-$) of MO and protonated amino functionalities present on the adsorbent surface. The cooperative effect of hydrogen bonding, π–π stacking, and electrostatic interactions provides multiple adsorption sites and stabilizes MO molecules at the solid–liquid interface. The different adsorption configurations of MB and MO reflect their contrasting molecular structures and charge distributions, demonstrating that Fe_2O_3/GSBA-15 offers versatile adsorption pathways capable of accommodating both cationic and anionic organic dyes.

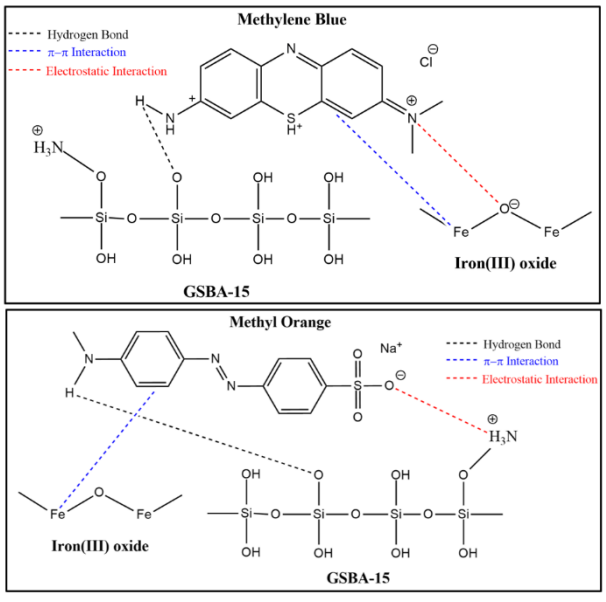

Figure 9. A schematic illustration describing interactions between dye molecules and Fe_2O_3/GSBA-15-TIE.

4. Conclusions

In this study, we present a cost-effective, one-step synthesis method for Fe_2O_3-doped GSBA-15 using tamarind pulp extract (TIE), a natural and sustainable organic activating agent. Our findings were thoroughly validated through various characterization techniques, including FTIR, XRD, SEM-EDX, and UV-Vis spectroscopy. FTIR analysis confirmed successful activation and impregnation, as evidenced by the distinct bonding peaks of bioorganic molecules from TIE and the Fe-O bonds, signifying the successful incorporation of iron oxide. XRD results suggested the presence of finely dispersed nano-sized iron oxide particles within the mesoporous structure. SEM-EDX analysis further demonstrated that iron oxide was effectively immobilized on GSBA-15, showing a characteristic rod-like morphology with particle agglomeration. Regarding adsorption performance, the GSBA-15 and Fe_2O_3/GSBA-15 TIE samples demonstrated notable capacities for methylene blue (MB) and methyl orange (MO) adsorption. At the optimal adsorption time, the Fe_2O_3/GSBA-15 TIE composite achieved a capacity of 183.497 $mg.g^{-1}$ for MB, compared to 176.062 $mg.g^{-1}$ for pure GSBA-15, and 16 $mg.g^{-1}$ for MO, a slight increase over the 15.582 $mg.g^{-1}$ of pure GSBA-15. These results highlight the potential of Fe_2O_3/GSBA-15 TIE as an effective material for dye adsorption, with promising implications for sustainable environmental solutions. The successful synthesis of Fe_2O_3/GSBA-15 using TIE not only enhances the material's adsorption capacity but also demonstrates the feasibility of using eco-friendly, natural activators in the development of advanced mesoporous silica composites. This approach presents a novel and environmentally benign alternative to conventional methods, offering a promising strategy for addressing future environmental challenges related to wastewater treatment and pollutant removal.

Acknowledgment

The authors gratefully acknowledge the financial support provided by Universitas Sebelas Maret through the Penelitian Unggulan Terapan A (PUTA UNS) funding scheme under Contract No. 460/UN27.22/PT.01.03/2026.

CRedit Author Statement

Author Contributions: Maria Ulfa: Conceptualization, Methodology, Investigation, Validation, Data curation, Writing – original draft, Writing – review & editing, Supervision, Project administration, and Funding acquisition. Youlanda Jesiva Alba: Investigation, Experimental work, Data curation, Formal

analysis, and Visualization. Nurma Yunita Indriyanti: Investigation, Characterization, Data analysis, Validation, and Visualization. Nanik Dwi Nurhayati: Methodology, Validation, Resources, Writing – review & editing, and Supervision. Agung C. Saputro: Methodology, Formal analysis, Validation, Resources, Writing – review & editing, and Supervision. All authors have read and agreed to the published version of the manuscript.

References

[1] Alex Mbachu, C., Kamoru Babayemi, A., Chinedu Egbosiuba, T., Ifeanyichukwu Ike, J., Jacinta Ani, I., Mustapha, S. (2023). Green synthesis of iron oxide nanoparticles by Taguchi design of experiment method for effective adsorption of methylene blue and methyl orange from textile wastewater. *Results in Engineering*, 19, 101198. DOI: 10.1016/j.rineng.2023.101198.

[2] Islam, T., Repon, M.R., Islam, T., Sarwar, Z., Rahman, M.M. (2023). Impact of textile dyes on health and ecosystem: a review of structure, causes, and potential solutions. *Environmental Science and Pollution Research*, 30, 9207–9242. DOI: 10.1007/s11356-022-24398.

[3] Sagadevan, S., Fatimah, I., Egbosiub, T.C., Alshahateet, S.F., Lett, J.A., Weldegebrieal, G.K., Le, M.V., Johan, M.R. (2022). Photocatalytic Efficiency of Titanium Dioxide for Dyes and Heavy Metals Removal from Wastewater. *Bulletin of Chemical Reaction Engineering and Catalysis*, 17(2), 430–450. DOI: 10.9767/bcrec.17.2.13948.430-450.

[4] Qureshi, S.S., Shah, V., Nizamuddin, S., Mubarak, N.M., Karri, R.R., Dehghani, M.H., Ramesh, S., Khalid, M., Rahman, M.E. (2022). Microwave-assisted synthesis of carbon nanotubes for the removal of toxic cationic dyes from textile wastewater. *Journal of Molecular Liquids*, 356, 119045. DOI: 10.1016/j.molliq.2022.119045.

[5] Chinedu Egbosiuba, T. (2022). Application of Agricultural Waste in Anionic Dyes Removal from Wastewater. In: *Sustainable Textiles: Production, Processing, Manufacturing and Chemistry,* 2, 111–141. DOI: 10.1007/978-981-19-2852-9_7.

[6] Rajendran, J., Panneerselvam, A., Ramasamy, S., Palanisamy, P. (2024). Methylene blue and methyl orange removal from wastewater by magnetic adsorbent based on activated carbon synthesised from watermelon shell. *Desalination and Water Treatment*, 317, 100040. DOI: 10.1016/j.dwt.2024.100040.

[7] Boukoussa, B., Hakiki, A., Nunes-Beltrao, A.P., Hamacha, R., Azzouz, A. (2018). Assessment of the intrinsic interactions of nanocomposite polyaniline/SBA-15 with carbon dioxide: Correlation between the hydrophilic character and surface basicity. *Journal of CO2 Utilization*, 26, 171–178. DOI: 10.1016/j.jcou.2018.05.006.

[8] Sabri, A.A., Albayati, T.M., Alazawi, R.A. (2015). Synthesis of ordered mesoporous SBA-15 and its adsorption of methylene blue. *Korean Journal of Chemical Engineering*, 32(9), 1835–1841. DOI: 10.1007/s11814-014-0390-y.

[9] Trisunaryanti, Wega., T. (2022). Katalis Cerdas Bermatriks Material Mesopori Tercetak Gelatin: Sintesis dan Aplikasinya. UGM PRESS.

[10] Ulfa, M., Setiarini, I. (2022). The Effect of Zinc Oxide Supported on Gelatin Mesoporous Silica (GSBA-15) on Structural Character and Their Methylene Blue Photodegradation Performance. *Bulletin of Chemical Reaction Engineering & Catalysis*, 17(2), 363-374. DOI: 10.9767/bcrec.17.2.13712.363-374.

[11] Sachithanadam, M., Joshi, S.C. (2014). A New Phenomenon of Compressive Strain Recovery in Gelatin-silica Aerogel Composites with SDS. *Procedia Engineering*, 75, 51–55. DOI: 10.1016/j.proeng.2013.11.010.

[12] Ulfa, M., Prasetyoko, D., Mahadi, A.H., Bahruji, H. (2020). Size tunable mesoporous carbon microspheres using Pluronic F127 and gelatin as co-template for removal of ibuprofen. *Science of the Total Environment*, 711, 135066. DOI: 10.1016/j.scitotenv.2019.135066.

[13] Ulfa, M., Prasetyoko, D., Trisunaryanti, W., Bahruji, H., Fadila, Z.A., Sholeha, N.A. (2022). The effect of gelatin as pore expander in green synthesis mesoporous silica for methylene blue adsorption. *Scientific Reports*, 12(1), 15271. DOI: 10.1038/s41598-022-19615-5.

[14] Ulfa, M., Istanti, S.A. (2022). Synthesis of Mesoporous Silica Incorporated with Low Iron Concentration and Gelatin Co-Template via The Ultrasonication Method and Its Methylene Blue Photodegradation Performance. *Bulletin of Chemical Reaction Engineering & Catalysis*, 17(4), 831–838. DOI: 10.9767/bcrec.17.4.16210.831-838.

[15] Cashin, V.B., Eldridge, D.S., Yu, A., Zhao, D. (2018). Surface functionalization and manipulation of mesoporous silica adsorbents for improved removal of pollutants: A review. *Environmental Science: Water Research & Technology*. 4(2), 110–128. DOI: 10.1039/c7ew00322f.

[16] Arshad, M.S., Imran, M., Ahmed, A., Sohaib, M., Ullah, A., Nisa, M. un, Hina, G., Khalid, W., Rehana, H. (2019). Tamarind: A diet-based strategy against lifestyle maladies. *Food Sci. Nutr*. 7(11), 3378–3390. DOI: 10.1002/fsn3.1218.

[17] Rápó, E., Tonk, S. (2021). Factors affecting synthetic dye adsorption; desorption studies: A review of results from the last five years (2017–2021). *Molecules*, 26, 26(17), 5419. DOI: 10.3390/molecules26175419.

[18] Guo, X., Zhao, Z., Gao, X., Dong, Y., Fu, H., Zhang, X. (2024). Study on the adsorption performance of modified high silica fly ash for methylene blue. *RSC Advances*, 14(30), 21342–21354. DOI: 10.1039/d4ra04017a.

[19] Yadav, B.S., Dasgupta, S. (2022). Effect of time, pH, and temperature on kinetics for adsorption of methyl orange dye into the modified nitrate intercalated MgAl LDH adsorbent. *Inorg. Chem. Commun.* 137, 109203. DOI: 10.1016/j.inoche.2022.109203.

[20] Flores, D., Almeida, C.M.R., Gomes, C.R., Balula, S.S., Granadeiro, C.M. (2023). Tailoring of Mesoporous Silica-Based Materials for Enhanced Water Pollutants Removal. *Molecules*, 28(10), 4038. DOI: 10.3390/molecules28104038.

[21] Khan, M.D., Singh, A., Khan, M.Z., Tabraiz, S., Sheikh, J. (2023). Current perspectives, recent advancements, and efficiencies of various dye-containing wastewater treatment technologies. *Journal of Water Process Engineering*, 53(7), 103579. DOI: 10.1016/j.jwpe.2023.103579.

[22] Astuti, E., Mufrodi, Z., Amelia, S., Zulfi, M.I., Ramadhani, F. (2023). Production of Activated Carbon by Activation of Tamarind (Tamarindus Indica) Wood Charcoal. *CHEMICA: Jurnal Teknik Kimia*, 10(1) DOI: 10.26555/chemica.v10i1.25260.

[23] Riyad, Y.M., Elmorsi, T.M., Alam, M.G., Abel, B. (2023). Surface Functionalization of Bioactive Hybrid Adsorbents for Enhanced Adsorption of Organic Dyes. *International Journal of Environmental Research and Public Health*, 20(9), 5750. DOI: 10.3390/ijerph20095750.

[24] Zheng, H., Schenk, J., Spreitzer, D., Wolfinger, T., Daghagheleh, O. (2021). Review on the Oxidation Behaviors and Kinetics of Magnetite in Particle Scale. *Steel Res. Int.* 92(8), 2000687. DOI: 10.1002/srin.202000687.

[25] Tukan, D.N., Rosmainar, L., Kustomo, K., Rasidah, R. (2023). A Review: Optimum Conditions for Magnetite Synthesis (Fe3O4). *Jurnal Berkala Ilmiah Sains dan Terapan Kimia*, 17(2), 15–21. DOI: 10.20527/jstk.v17i2.15134.

[26] Foroutan, R., Peighambardoust, S.J., Peighambardoust, S.H., Pateiro, M., Lorenzo, J.M. (2021). Adsorption of crystal violet dye using activated carbon of lemon wood and activated carbon/fe3 o4 magnetic nanocomposite from aqueous solutions: A kinetic, equilibrium and thermodynamic study. *Molecules*, 26(8), 2241. DOI: 10.3390/molecules26082241.

[27] Phuong Ha, L., Van Ngoc, N., Trang Huyen, N.T., Thu Hang, L.T., Kieu Oanh, N.T., Tuyet, T.T., Mai Phuong, N.T., Minh Hong, N.T. (2022). Total phenolic, flavonoid contents and antioxidant activity of tamarind seed and pulp extracts. *Vietnam Journal of Biotechnology*, 20(2), 305–316. DOI: 10.15625/1811-4989/15930.

[28] Ulfa, M., Miftahul Jannah, A. (2018). Synthesis of Mesoporous Fe2O3/SBA-15 and its Application for Nickel (II) Ion Adsorption. *Oriental Journal of Chemistry*, 34(1), 420–427. DOI: 10.13005/ojc/340145.

[29] Thatikayala, D., Banothu, V., Kim, J., Shin, D.S., Vijayalakshmi, S., Park, J. (2020). Enhanced photocatalytic and antibacterial activity of ZnO/Ag nanostructure synthesized by Tamarindus indica pulp extract. *Journal of Materials Science: Materials in Electronics*, 31(7), 5324–5335. DOI: 10.1007/s10854-020-03093-4.

[30] McCool, B., Murphy, L., Tripp, C.P. (2006). A simple FTIR technique for estimating the surface area of silica powders and films. *Journal of Colloid and Interface Science*, 295(1), 294–298. DOI: 10.1016/j.jcis.2005.08.010.

[31] Salama, R.S., El-Bahy, S.M., Mannaa, M.A. (2021). Sulfamic acid supported on mesoporous MCM-41 as a novel, efficient and reusable heterogenous solid acid catalyst for synthesis of xanthene, dihydropyrimidinone and coumarin derivatives. *Colloids and Surfaces A: Physicochemical and Engineering Aspects*, 628, 127261. DOI: 10.1016/j.colsurfa.2021.127261.

[32] Faaizatunnisa, N., Lestari, W.W., Saputra, O.A., Saraswati, T.E., Larasati, L., Wibowo, F.R. (2022). Slow-Release of Curcumin Induced by Core–Shell Mesoporous Silica Nanoparticles (MSNs) Modified MIL-100(Fe) Composite. *Journal of Inorganic and Organometallic Polymers and Materials*, 32(5), 1744–1754. DOI: 10.1007/s10904-022-02230-2.

[33] Zeleňáková, A., Hrubovčák, P., Kapusta, O., Kučerka, N., Kuklin, A., Ivankov, O., Zeleňák, V. (2019). Size and distribution of the iron oxide nanoparticles in SBA-15 nanoporous silica via SANS study. *Scientific Reports*, 9(1), 15852. DOI: 10.1038/s41598-019-52417-w.

[34] Lycourghiotis, S., Makarouni, D., Kordouli, E., Bourikas, K., Kordulis, C., Dourtoglou, V. (2018). Activation of natural mordenite by various acids: Characterization and evaluation in the transformation of limonene into p-cymene. *Molecular Catalysis*, 450, 95–103. DOI: 10.1016/j.mcat.2018.03.013.

[35] Raja, P.B., Munusamy, K.R., Perumal, V., Ibrahim, M.N.M. (2021). Characterization of nanomaterial used in nanobioremediation. In: *Nano-Bioremediation: Fundamentals and Applications,* 57–83. DOI: 10.1016/B978-0-12-823962-9.00037-4.

[36] Lagergren, S. (1898). About the theory of so-called adsorption of soluble substances (Zur theorie der sogenannten adsorption geloster stoffe) Kungliga Svenska Vetenskapsakademiens. *Handlingar*, 24(4), 1–39.

[37] Ho, Y.S., McKay, G. (1999). Pseudo-second order model for sorption processes. *Process Biochemistry*, 34(5), 451–465. DOI: 10.1016/S0032-9592(98)00112-5.

[38] Sağ, Y., Aktay, Y. (2002). Kinetic studies on sorption of Cr(VI) and Cu(II) ions by chitin, chitosan and Rhizopus arrhizus. *Biochemical Engineering Journal*, 12(2), 143–153. DOI: 10.1016/S1369-703X(02)00068-2.

[39] Kwon, S., Fan, M., DaCosta, H.F.M., Russell, A.G., Berchtold, K.A., Dubey, M.K. (2011). CO2 Sorption. In: *Coal Gasification and Its Applications*. Elsevier, pp. 293–339. DOI: 10.1016/B978-0-8155-2049-8.10010-5.

[40] Meechai, T., Poonsawat, T., Limchoowong, N., Laksee, S., Chumkaeo, P., Tuanudom, R., Yatsomboon, A., Honghernsthit, L., Somsook, E., Sricharoen, P. (2023). One-pot synthesis of iron oxide - Gamma irradiated chitosan modified SBA-15 mesoporous silica for effective methylene blue dye removal. *Heliyon*, 9(5), e16178. DOI: 10.1016/j.heliyon.2023.e16178.